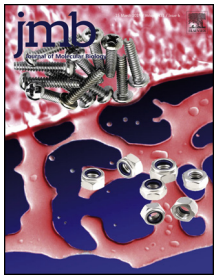

Force-Profile Analysis of the Cotranslational Folding of HemK and Filamin Domains: Comparison of Biochemical and Biophysical Folding Assays

Grant Kemp [1,†], Renuka Kudva [1,†], Andrés de la Rosa [1] and Gunnar von Heijne [1,2]

*1 - **Department of Biochemistry and Biophysics,** Stockholm University, SE-106 91 Stockholm, Sweden*
*2 - **Science for Life Laboratory,** Stockholm University, Box 1031, SE-171 21 Solna, Sweden*

***Correspondence to Gunnar von Heijne:** Department of Biochemistry and Biophysics, Stockholm University, SE-106 91 Stockholm, Sweden. gunnar@dbb.su.se*
https://doi.org/10.1016/j.jmb.2019.01.043
Edited by Sheena Radford

Abstract

We have characterized the cotranslational folding of two small protein domains of different folds—the α-helical N-terminal domain of HemK and the β-rich FLN5 filamin domain—by measuring the force that the folding protein exerts on the nascent chain when located in different parts of the ribosome exit tunnel (force-profile analysis, or FPA), allowing us to compare FPA to three other techniques currently used to study cotranslational folding: real-time FRET, photoinduced electron transfer, and NMR. We find that FPA identifies the same cotranslational folding transitions as do the other methods, and that these techniques therefore reflect the same basic process of cotranslational folding in similar ways.

In recent years, a number of new experimental methods for analyzing the cotranslational folding of protein domains have been developed. These include real-time FRET analysis [1] and methods in which nascent polypeptide chains of defined lengths are arrested in the ribosome and their folding status analyzed by, for example, cryo-EM [2,3], protease resistance [1,4–9], NMR [10–15], photoinduced electron transfer (PET) [1,16], folding-associated cotranslational sequencing [17], optical tweezer pulling [18–21], fluorescence measurements [22], and measuring the force that the folding protein exerts on the nascent chain using a translational arrest peptide (AP) as a force sensor [2,3,9,21,23–25]. Furthermore, coarse-grained molecular dynamic simulations of various flavors can provide detailed insights into cotranslational folding reactions [26–30], especially when coupled with experimental studies [3,26,31].

While these different methods have all been used with success, they have rarely been directly compared on the same target protein. As a first step toward such comparisons, we now report AP-based force-profile analysis (FPA) for two protein domains—the α-helical HemK N-terminal domain (HemK-NTD) and the β-sheet-rich FLN5 filamin domain—that have previously been studied by real-time FRET/PET and NMR, respectively [1,14,16]. We find that FPA identifies the same cotranslational folding transitions as do the other methods. We conclude that results obtained with the different methods can be interpreted under a common conceptual framework, albeit at different levels of detail and with different limitations inherent to the analysis.

AP-Based Force Profiles

FPA is based on the observation that the efficiency of AP-induced translational stalling is reduced when the nascent chain is subject to an external pulling force [21,32,33]. As shown in Fig. 1, such a pulling force can be induced by cotranslational protein folding. For constructs where the tether + AP segment is long enough that there is just enough space in the ribosome exit tunnel for the protein to fold if the segment is stretched out from its equilibrium length, some of the free energy gained upon folding will be stored as elastic energy (increased tension) in the nascent chain, reducing stalling and increasing the relative amount of full-length protein (Fig. 1a). By measuring the stalling efficiency (measured as fraction full-length protein, f_{FL}) for a series of constructs of increasing tether length

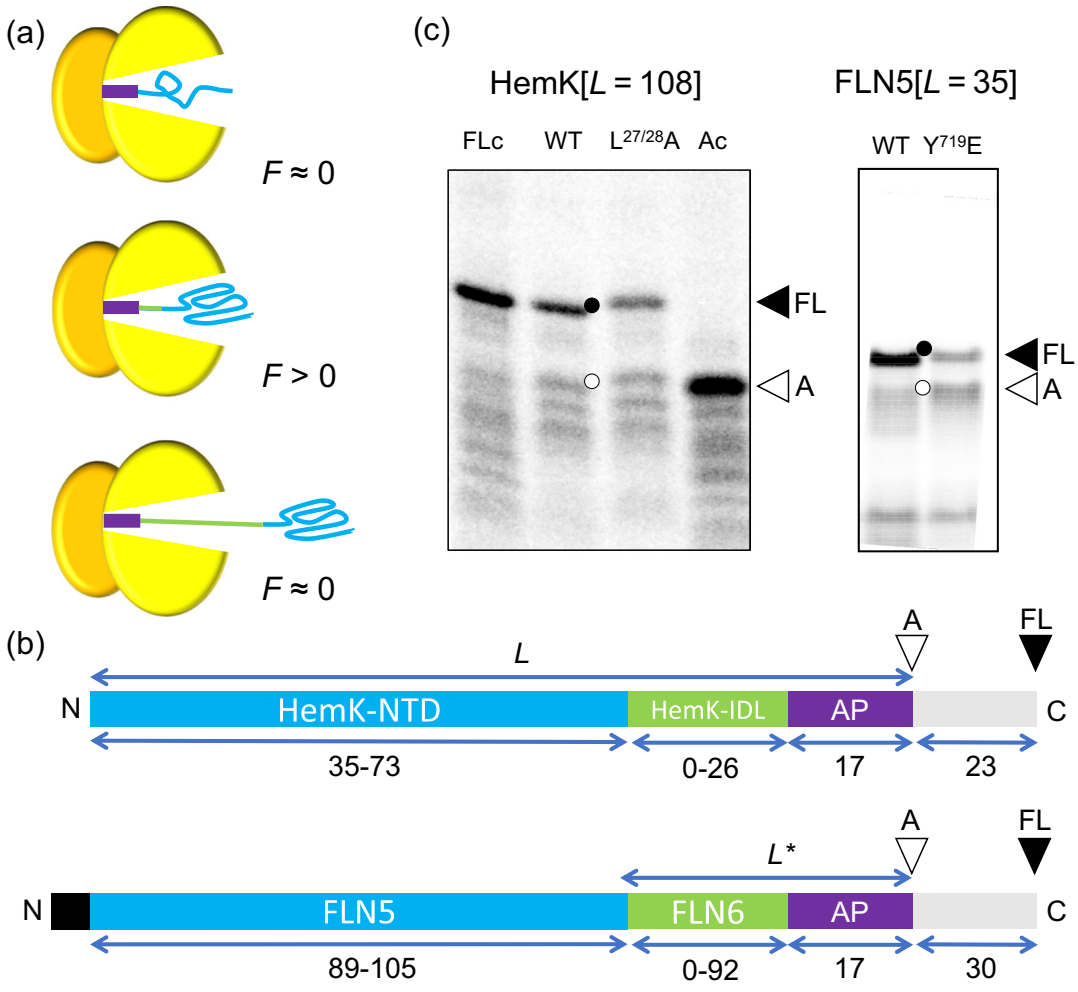

Fig. 1. The FPA assay. (a) Cotranslational folding can generate force on the nascent chain. The nascent protein is in blue, the tether in green, the AP in purple, and the ribosomal subunits in yellow. At short tether lengths, the protein is still too deep in the exit tunnel to fold when the AP is reached, there is negligible force exerted on the stalled nascent chain ($F \approx 0$, top panel), and the arrested (*A*) form of the protein is the main product. Similarly, at long tether lengths, the protein is already folded when the AP is reached, little force is exerted ($F \approx 0$, bottom panel), and mostly *A* is produced. However, at some intermediate tether length when there is just enough space in the exit tunnel for the protein to fold if the tether is stretched, force will be exerted on the nascent chain ($F > 0$, middle panel), reducing stalling and increasing the amount of full-length (*FL*) product. (b) Schematic representation of the HemK and FLN5 constructs (full sequences can be found in Supplementary Table 1). HemK-NTD (and its truncations) or FLN5 (blue) was tethered to the SecM(*Ec*) AP (purple) by a varying length parts of their respective native downstream sequence (green), either the HemK interdomain linker (HemK-IDL) or the FLN6 filamin domain. Following the AP, a sequence of 23 (for HemK) or 30 (for FLN5) amino acids derived from LepB is included to allow the resolution of arrested (*A*) or full length (*FL*) products by SDS-PAGE (empty and filled triangles, respectively). The HemK-IDL was progressively truncated from its C-terminal end from 26 down to 0 residues, followed by truncation of HemK-NTD from 73 down to 35 residues, as indicated by the numbers underneath the cartoon representations. Likewise, the FLN6 linker segment was truncated from its C-terminal end from 92 down to 0 residues, followed by truncation of FLN5 from 105 down to 89 residues. (c) SDS-PAGE of the *in vitro* translation products of the HemK[*L* = 108] (left) and FLN5[*L* = 35] (right) with arrested (*A*) and full-length (*FL*) products indicated. HemK[*L* = 108]: lane 1, full-length control (FLc) construct where the C-terminal, critical Pro of the SecM(*Ec*) AP is substituted by Ala, which eliminates arrest; lane 2, wild-type construct; lane 3, unstable mutant $L^{27}A + L^{28}A$; lane 4, arrest control (Ac) construct where the codon immediately following the AP has been mutated to a TAA stop codon. FLN5[*L* = 35]: lane 1, wild-type FLN5[*L* = 35] construct; lane 2, non-folding mutant control $Y^{719}E$. Materials and Methods are available as a Supplement.

(Fig. 1b, c), a force profile can be generated that shows how the folding force varies with the location of the protein in the exit tunnel [2], and hence when during translation the protein starts to fold. FPA has been used to map the cotranslational folding of more than 10 different proteins so far [9].

Cotranslational Folding of the HemK N-Terminal Domain

In a pioneering study, Holtkamp *et al.* [1] followed the cotranslational folding of the 73-residue long HemK-NTD (Fig. 2a) in real time using both FRET- and PET-based assays. A subsequent, more detailed analysis [16] led to the identification of four folding intermediates (I–IV) in addition to the native state (V), which were proposed to correspond to the linear, stepwise addition of individual α-helices to a growing, compact core. Furthermore, it was concluded that the folding reaction is rate-limited by translation (which proceeds at a rate of ~4 codons s^{-1} in the *in vitro* translation system used [1]). A coarse-grained molecular dynamics study has also provided evidence for the cotranslational appearance of compact folding intermediates composed of the first three (intermediate II) and first four (intermediate III) α-helices of HemK-NTD, followed by de-compaction (intermediate IV) and folding into the native 5-helix bundle (V) at longer tether lengths [26].

In order to compare FPA to the FRET and PET assays, we recorded a force profile for HemK-NTD at ~5-residue resolution using the *Escherichia coli* SecM(*Ec*) AP, Fig. 2b (red curve; in this case, in order to be consistent with the previous publications [1,16], we measured *L* from the N-terminus of HemK-NTD to the C-terminal end of the AP, Fig. 1b). Four peaks (A–D) are apparent in the force profile. Peak D ($L \approx 100$–110 residues) coincides with the formation of the native state V as seen by FRET, and corresponds to a situation where the C-terminal end of HemK-NTD is 30–35 residues away from the ribosome peptidyl transferase centre, close to the exit-port region where other proteins of similar size have been found to fold into their native state [3,24]. Strikingly, peaks A–C in the force profile nicely match the folding intermediates I–III identified by real-time FRET and PET analysis [16], although peak B is just barely detectable above the background. The proposed intermediate IV is not resolved in the force profile, but may contribute to the early shoulder of peak D.

To test how mutations in the hydrophobic core of HemK-NTD affect the observed forces, we recorded a force profile for a mutant HemK-NTD in which $Leu^{27}$and Leu^{28} in helix H2 were simultaneously mutated to Ala (Fig. 2a, and blue curve in Fig. 2b). The $L^{28}A$ mutation reduces the *in vitro* denaturation temperature of HemK-NTD from 50 °C to 30 °C [1]. The [$L^{27}A$ + $L^{28}A$] mutation caused a strong reduction of the amplitude of peak D, but had only marginal effects on peaks A and C. Interestingly, the mutation led to a marked increase the amplitude of peak B. To confirm these effects, we also measured f_{FL} values for a Leu^{7} to Asn mutation in helix H1 (Fig. 2a) for *L* values corresponding to peaks A–D. As seen in Fig. 2c, the $L^{7}N$ mutation behaves similarly to the [$L^{27}A$ + $L^{28}A$] mutation: f_{FL} is strongly reduced for peak D, not affected for peaks A and C, and increased for peak B.

Finally, we also recorded an *in vivo* force profile by expression of the HemK-NTD constructs in *E. coli* cells. An HA tag was added just before the AP to enable the detection of HemK-NTD translation products by immunoprecipitation. Guided by previous mutagenesis studies of a SecM AP [35], we placed the HA tag overlapping the SecM(*Ec*) AP, resulting in an HA-AP sequence that was of the same length and somewhat lower stalling strength than the SecM(*Ec*) AP used in the *in vitro* experiments (Supplementary Fig. S1). The HemK-NTD force profile obtained *in vivo* (Fig. 2b, green curve) is similar to the one obtained *in vitro* (Fig. 2b, red curve), although peaks A and D are shifted to somewhat lower *L* values. Considering the lack of chaperones such as trigger factor and GroEL/ES in the PURE *in vitro* translation system and the ~20-fold faster translation rate *in vivo*, the correspondence between the *in vitro* and *in vivo* force profiles is remarkably good.

We conclude that FRET/PET, MD, and FPA all give similar a similar picture of the cotranslational folding of HemK-NTD, and all detect the formation of at least two folding intermediates as well as the native state. Mutation of residues in the hydrophobic core of HemK-NTD reduces the amplitude of peak D (corresponding to the native state) in the force profile as expected, but has little effect on peaks A and C and even increases the amplitude of peak B, suggesting that the corresponding folding intermediates may have less well-defined tertiary structures than the native fold and hence be less sensitive to individual point-mutations.

Cotranslational Folding of the FLN5 Domain

The cotranslational folding of the Ig-like FLN5 filamin domain has previously been studied by NMR measurements on ribosome-attached nascent chains and of purified C-terminally truncated versions of the protein [13,14]. The main conclusion from these studies is that FLN5 folds only when it has fully cleared the exit tunnel and is some distance away from the ribosome surface, at a tether length of 40–45 residues. This tether length is clearly longer than what is required for folding of a similar-sized Ig-like domain such as the I27 titin domain that folds at a tether length of ~35 residues, as determined by FPA and cryo-EM [3]. The simplest explanation for the long tether length required for cotranslational folding of FLN5 is that the ribosome surface destabilizes the folded state relative to the unfolded state [14], as has been observed for other proteins when tethered to a ribosome [20,36,37].

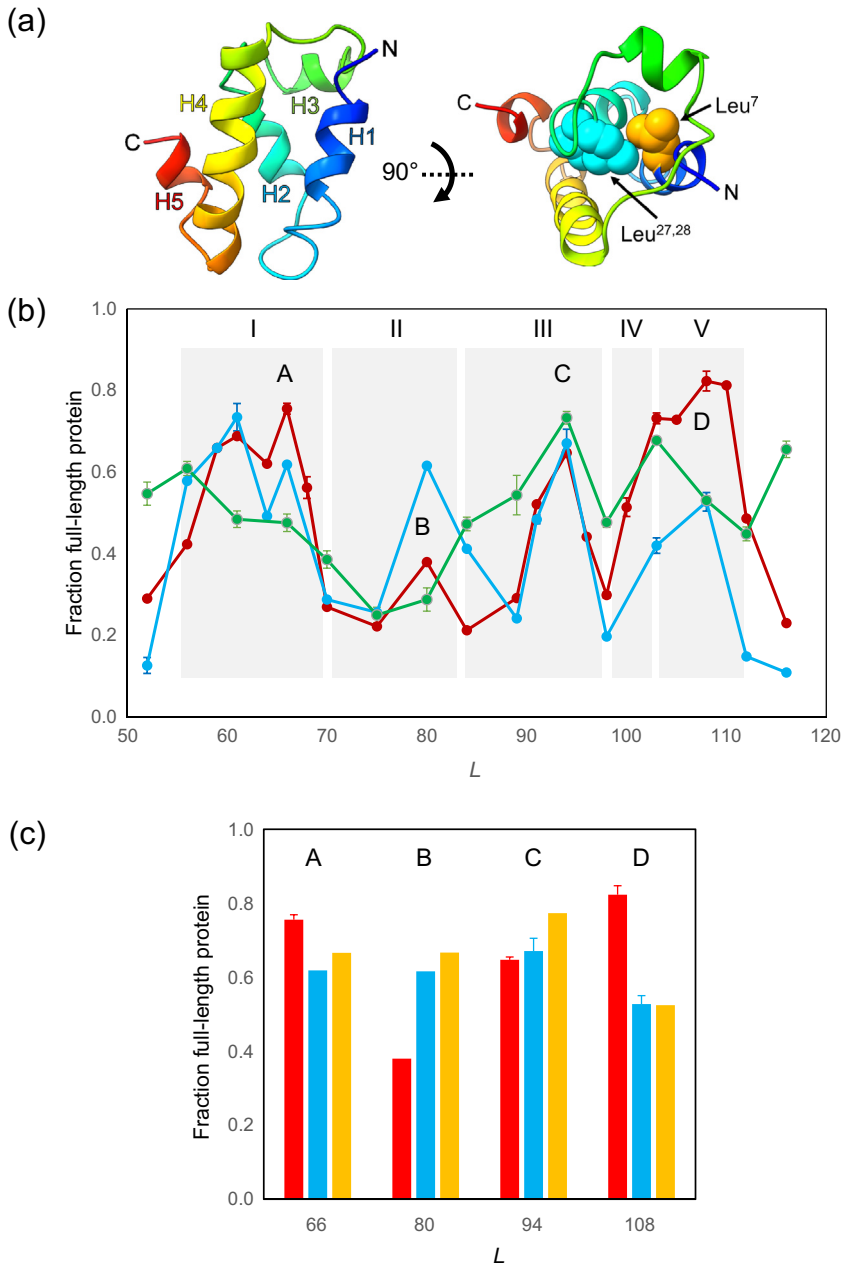

Fig. 2. FPA of Hemk-NTD using the SecM(*Ec*) AP as the force sensor. (a) Ribbon representation of the backbone structure of HemK-NTD (PDB 1T43 [34]) rainbow colored from the N-terminus (blue) to the C-terminus (red) showing the five α-helices (H1-H5). Leu^{7} (orange), Leu^{27}, and Leu^{28} (blue) are shown as spheres. (b) Force profiles obtained by translation in the *E. coli*-derived PURE *in vitro* transcription–translation system (red curve), by *in vivo* expression in *E. coli* (green curve), and by *in vitro* expression of the unstable $L^{27,28}A$ mutant (blue curve). Peaks in the force profile discussed in the text are labeled A–D. The shaded areas labeled I–V indicate the approximate *L* values corresponding to the folding intermediates (I–IV) and the native structure (V) derived from real-time FRET/PET measurements [1,16]. *L* is the number of residues between the N-terminal end HemK-NTD and the C-terminal residue of the AP (c.f., Fig. 1b). (c) f_{FL} values for wild-type HemK-NTD (red), the $L^{27}A+ L^{28}A$ mutant (blue), and the $L^{7}N$ (orange) mutant at *L* = 66, 80, 94, and 110 residues (corresponding to peaks A–D in the force profile in panel *a*, as indicated). Error bars indicate SEM values.

Given that the NMR data indicate that FLN5 folds at a considerably longer tether length than I27, we were curious to see if this is also reflected in its force profile. The FLN5 force profile obtained with a mutant AP, SecM(*Ec*, S → K) (see Supplementary Materials and Methods), that is somewhat more resistant to pulling force than is SecM(*Ec*) is shown in Fig. 3, together with a curve derived from the NMR

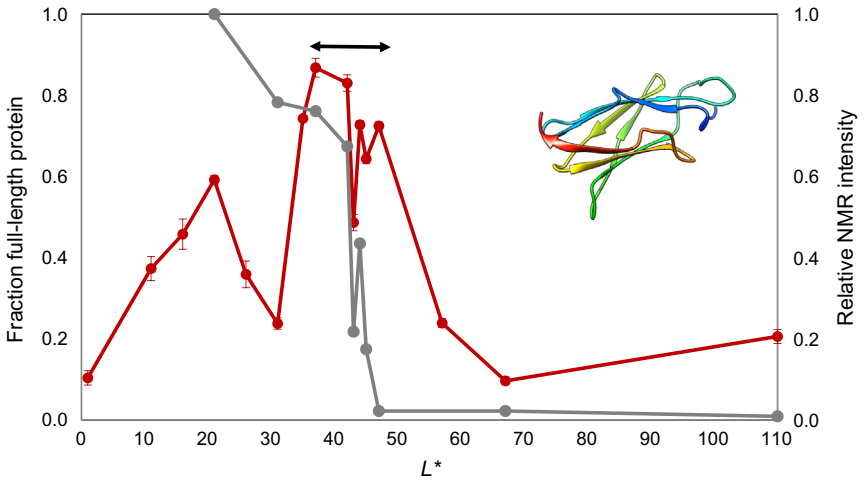

Fig. 3. FPA of FLN5 using the SecM(*Ec*, S → K) AP as the force sensor (red curve) and averaged relative NMR intensities of three ^{15}N amide resonances arising from the unfolded FLN5 domain (gray curve) [14] as a function of L^*. The force profile was obtained by *in vitro* translation in the *E. coli*-derived PURE *in vitro* transcription–translation system. Error bars indicate SEM values. The arrow indicates the location of the folding transition derived from the NMR data. L^* is the number of residues between the C-terminal end of the FLN5 domain and the C-terminal residue of the AP (c.f., Fig. 1b). Inset: ribbon representation of the backbone structure of FLN5 (PDB 2N62), colored from N-terminus (blue) to C-terminus (red).

data showing averaged relative intensities of three ^{15}N amide resonances arising from the unfolded FLN5 domain [14]. To be consistent with the published NMR data [13,14], in this case, we plot the data as a function of L^*, that is, the distance between the C-terminal end of the FLN5 domain and the peptidyl transferase centre (c.f., Fig. 1b). The force profile has two peaks: one at $L^* = 35$–47 residues that coincides with the main folding transition detected by NMR and one at $L^* \approx 20$ residues. There is an apparently significant dip both in the force profile and the NMR profile at $L^* = 43$ residues; at present, we have no explanation for this precisely localized feature in the two profiles.

To validate that the main peak at $L^* = 35$–47 residues in the force profile reflects folding into the native state, we also analyzed an unstable mutant of FLN5, Y^{719}E, using the weaker SecM(*Ec*) AP. As expected, the main peak is of significantly lower amplitude in this mutant; notably, however, the peak at $L^* \approx 20$ residues is unaffected (Supplementary Fig. S2 blue curve), mirroring the insensitivity of the early peaks in the HemK-NTD force profile to the [L^{27}A + L^{28}A] mutation (Fig. 2b).

The peak in the force profile at $L^* = 35$–47 residues is somewhat wider than the folding transition detected by NMR. Presumably, this is because the NMR resonances reflect only the folding transition itself, whereas the force profile reflects forces generated not only by the folding transition, but also by, for example, the folded protein when tethered close to the ribosome surface [38]. In line with this, the peak in the force profile extends to higher L^* values when the weaker SecM(*Ec*) AP is used (Supplementary Fig. S2).

In conclusion, the main cotranslational folding transition of FLN5 to the native state is detected both by NMR and FPA, and a putative folding intermediate is also apparent in the FPA data.

Summary

We have characterized the cotranslational folding of two small protein domains of different folds—the α-helical HemK-NTD and the β-rich FLN5—by FPA, allowing us to compare FPA to three other techniques currently used to study cotranslational folding: real-time FRET, PET, and NMR. The results show broad agreement between FPA on the one hand, and the three biophysical techniques on the other. Previously, we have shown that FPA also agrees with results from on-ribosome pulse-proteolysis [9] and coarse-grained MD simulations [2,3,39].

It thus appears that all these techniques reflect the same basic process of cotranslational folding in similar, yet distinct ways. FPA differs from the other presently used techniques in that it reflects not only the cotranslational folding process *per se* but in principle also other forces such as that expected to be generated when a folded protein is tethered close to the ribosome surface [38]. Our results nevertheless indicate that the methods discussed here can be expected to yield comparable results, at least for proteins that fold fast relative to the rate of translation. For proteins that fold more slowly, methods such as NMR, PET, pulse proteolysis, and FPA that are based on an analysis of nascent chains stably tethered to the ribosome may indicate folding at somewhat shorter tether lengths than will methods such as real-time

FRET, in which the nascent chain is being continuously lengthened during the assay [40].

Techniques that use stable tethering can potentially yield folding profiles with single-residue resolution, since the nascent chain can be lengthened one residue at a time. Real-time techniques, in contrast, average over a population of elongating ribosome–nascent chain complexes and further depend on an estimate of the local translation rate to convert from time to nascent chain length, and therefore cannot achieve single-residue resolution. It is still an open question as to what extent the fine structure of single-residue resolution data can yield useful information on the folding process.

It is particularly interesting to note that all the techniques appear able to detect intermediates on the cotranslational folding pathway, not just the formation of the native state. In-depth analysis of cotranslational folding intermediates may shed further light on how the presence of the ribosome affects protein folding.

Supplementary data to this article can be found online at https://doi.org/10.1016/j.jmb.2019.01.043.

Acknowledgments

FLN5 constructs previously used for NMR studies were kindly provided by Lisa Cabrita and John Christodoulou, University College London. This work was supported by grants from the Knut and Alice Wallenberg Foundation (2012.0282), the Swedish Cancer Foundation (15 0888), and the Swedish Research Council (621-2014-3713) to G.v.H.

Received 14 November 2018;
Received in revised form 27 January 2019;
Accepted 29 January 2019
Available online 7 February 2019

Keywords:
cotranslational folding;
HemK;
FLN5;
arrest peptide

†G.K. and R.K. contributed equally to this work.

Abbreviations used:
PET, photoinduced electron transfer; AP, arrest peptide; FPA, force-profile analysis.

References

[1] W. Holtkamp, G. Kokic, M. Jäger, J. Mittelstaet, A.A. Komar, M.V. Rodnina, Cotranslational protein folding on the ribosome monitored in real time, Science 350 (2015) 1104–1107.

[2] O.B. Nilsson, R. Hedman, J. Marino, S. Wickles, L. Bischoff, M. Johansson, A. Muller-Lucks, F. Trovato, J.D. Puglisi, E.P. O'Brien, R. Beckmann, G. von Heijne, Cotranslational protein folding inside the ribosome exit tunnel, Cell Rep. 12 (2015) 1533–1540.

[3] P. Tian, A. Steward, R. Kudva, T. Su, P.J. Shilling, A.A. Nickson, J.J. Hollins, R. Beckmann, G. von Heijne, R.B. Best, J. Clarke, The folding pathway of an Ig domain is conserved on and off the ribosome, Proc. Natl. Acad. Sci. U. S. A. (2018), https://doi.org/10.1073/pnas.1810523115.

[4] J. Frydman, H. Erdjument-Bromage, P. Tempst, F.U. Hartl, Co-translational domain folding as the structural basis for the rapid de novo folding of firefly luciferase, Nat. Struct. Biol. 6 (1999) 697–705.

[5] D.A. Kelkar, A. Khushoo, Z. Yang, W.R. Skach, Kinetic analysis of ribosome-bound fluorescent proteins reveals an early, stable, cotranslational folding intermediate, J. Biol. Chem. 287 (2012) 2568–2578.

[6] A.V. Nicola, W. Chen, A. Helenius, Co-translational folding of an alphavirus capsid protein in the cytosol of living cells, Nat. Cell Biol. 1 (1999) 341–345.

[7] G. Zhang, M. Hubalewska, Z. Ignatova, Transient ribosomal attenuation coordinates protein synthesis and co-translational folding, Nat. Struct. Mol. Biol. 16 (2009) 274–280.

[8] A.J. Samelson, E. Bolin, S.M. Costello, A.K. Sharma, E.P. O'Brien, S. Marqusee, Kinetic and structural comparison of a protein's cotranslational folding and refolding pathways, Sci. Adv. 4 (2018), eaas9098.

[9] J.A. Farias-Rico, F. Ruud Selin, I. Myronidi, M. Frühauf, G. von Heijne, Effects of protein size, thermodynamic stability, and net charge on cotranslational folding on the ribosome, Proc. Natl. Acad. Sci. U. S. A. 115 (2018) E9280–E9287.

[10] A.M. Cassaignau, H.M. Launay, M.E. Karyadi, X. Wang, C.A. Waudby, A. Deckert, A.L. Robertson, J. Christodoulou, L.D. Cabrita, A strategy for co-translational folding studies of ribosome-bound nascent chain complexes using NMR spectroscopy, Nat. Protoc. 11 (2016) 1492–1507.

[11] A. Deckert, C.A. Waudby, T. Wlodarski, A.S. Wentink, X. Wang, J.P. Kirkpatrick, J.F. Paton, C. Camilloni, P. Kukic, C.M. Dobson, M. Vendruscolo, L.D. Cabrita, J. Christodoulou, Structural characterization of the interaction of alpha-synuclein nascent chains with the ribosomal surface and trigger factor, Proc. Natl. Acad. Sci. U. S. A. 113 (2016) 5012–5017.

[12] C. Eichmann, S. Preissler, R. Riek, E. Deuerling, Cotranslational structure acquisition of nascent polypeptides monitored by NMR spectroscopy, Proc. Natl. Acad. Sci. U. S. A. 107 (2010) 9111–9116.

[13] C.A. Waudby, T. Wlodarski, M.E. Karyadi, A.M.E. Cassaignau, S.H.S. Chan, A.S. Wentink, J.M. Schmidt-Engler, C. Camilloni, M. Vendruscolo, L.D. Cabrita, J. Christodoulou, Systematic mapping of free energy landscapes of a growing filamin domain during biosynthesis, Proc. Natl. Acad. Sci. U. S. A. 115 (2018) 9744–9749.

[14] L.D. Cabrita, A.M. Cassaignau, H.M. Launay, C.A. Waudby, T. Wlodarski, C. Camilloni, M.E. Karyadi, A.L. Robertson, X. Wang, A.S. Wentink, L.S. Goodsell, C.A. Woolhead, M. Vendruscolo, C.M. Dobson, J. Christodoulou, A structural ensemble of a ribosome-nascent chain complex during cotranslational protein folding, Nat. Struct. Mol. Biol. 23 (2016) 278–285.

[15] L.D. Cabrita, S.T. Hsu, H. Launay, C.M. Dobson, J. Christodoulou, Probing ribosome-nascent chain complexes produced in vivo by NMR spectroscopy, Proc. Natl. Acad. Sci. U. S. A. 106 (2009) 22239–22244.

[16] E. Mercier, M.V. Rodnina, Co-translational folding trajectory of the HemK helical domain, Biochemistry 57 (2018) 3460–3464.
[17] Y. Han, A. David, B. Liu, J.G. Magadan, J.R. Bennink, J.W. Yewdell, S.B. Qian, Monitoring cotranslational protein folding in mammalian cells at codon resolution, Proc. Natl. Acad. Sci. U. S. A. 109 (2012) 12467–12472.
[18] A. Katranidis, W. Grange, R. Schlesinger, T. Choli-Papadopoulou, D. Bruggemann, M. Hegner, G. Buldt, Force measurements of the disruption of the nascent polypeptide chain from the ribosome by optical tweezers, FEBS Lett. 585 (2011) 1859–1863.
[19] F. Wruck, A. Katranidis, K.H. Nierhaus, G. Buldt, M. Hegner, Translation and folding of single proteins in real time, Proc. Natl. Acad. Sci. U. S. A. 114 (2017) E4399–E4407.
[20] C.M. Kaiser, D.H. Goldman, J.D. Chodera, I. Tinoco Jr., C. Bustamante, The ribosome modulates nascent protein folding, Science 334 (2011) 1723–1727.
[21] D.H. Goldman, C.M. Kaiser, A. Milin, M. Righini, I. Tinoco, C. Bustamante, Mechanical force releases nascent chain-mediated ribosome arrest *in vitro* and *in vivo*, Science 348 (2015) 457–460.
[22] K.G. Ugrinov, P.L. Clark, Cotranslational folding increases GFP folding yield, Biophys. J. 98 (2010) 1312–1320.
[23] O.B. Nilsson, A. Müller-Lucks, G. Kramer, B. Bukau, G. von Heijne, Trigger factor reduces the force exerted on the nascent chain by a cotranslationally folding protein, J. Mol. Biol. 428 (2016) 1356–1364.
[24] O.B. Nilsson, A.A. Nickson, J.J. Hollins, S. Wickles, A. Steward, R. Beckmann, G. von Heijne, J. Clarke, Cotranslational folding of spectrin domains via partially structured states, Nat. Struct. Mol. Biol. 24 (2017) 221–225.
[25] J.A. Farias-Rico, S.K. Goetz, J. Marino, G. von Heijne, Mutational analysis of protein folding inside the ribosome exit tunnel, FEBS Lett. 591 (2017) 155–163.
[26] D.A. Nissley, E.P. O'Brien, Structural origins of FRET-observed nascent chain compaction on the ribosome, J. Phys. Chem. B 122 (2018) 9927–9937.
[27] E.P. O'Brien, J. Christodoulou, M. Vendruscolo, C.M. Dobson, New scenarios of protein folding can occur on the ribosome, J. Am. Chem. Soc. 133 (2011) 513–526.
[28] E.P. O'Brien, J. Christodoulou, M. Vendruscolo, C.M. Dobson, Trigger factor slows co-translational folding through kinetic trapping while sterically protecting the nascent chain from aberrant cytosolic interactions, J. Am. Chem. Soc. 134 (2012) 10920–10932.
[29] P. Ciryam, R.I. Morimoto, M. Vendruscolo, C.M. Dobson, E.P. O'Brien, *In vivo* translation rates can substantially delay the cotranslational folding of the *Escherichia coli* cytosolic proteome, Proc. Natl. Acad. Sci. U. S. A. 110 (2013) E132–E140.
[30] F. Trovato, E.P. O'Brien, Fast protein translation can promote co- and posttranslational folding of misfolding-prone proteins, Biophys. J. 112 (2017) 1807–1819.
[31] K.A. Merchant, R.B. Best, J.M. Louis, I.V. Gopich, W.A. Eaton, Characterizing the unfolded states of proteins using single-molecule FRET spectroscopy and molecular simulations, Proc. Natl. Acad. Sci. U. S. A. 104 (2007) 1528–1533.
[32] M.E. Butkus, L.B. Prundeanu, D.B. Oliver, Translocon "pulling" of nascent SecM controls the duration of its translational pause and secretion-responsive secA regulation, J. Bacteriol. 185 (2003) 6719–6722.
[33] N. Ismail, R. Hedman, N. Schiller, G. von Heijne, A biphasic pulling force acts on transmembrane helices during translocon-mediated membrane integration, Nat. Struct. Mol. Biol. 19 (2012) 1018–1022.
[34] Z. Yang, L. Shipman, M. Zhang, B.P. Anton, R.J. Roberts, X. Cheng, Structural characterization and comparative phylogenetic analysis of *Escherichia coli* HemK, a protein (N5)-glutamine methyltransferase, J. Mol. Biol. 340 (2004) 695–706.
[35] F. Cymer, R. Hedman, N. Ismail, G. von Heijne, Exploration of the arrest peptide sequence space reveals arrest-enhanced variants, J. Biol. Chem. 290 (2015) 10208–10215.
[36] A.J. Samelson, M.K. Jensen, R.A. Soto, J.H. Cate, S. Marqusee, Quantitative determination of ribosome nascent chain stability, Proc. Natl. Acad. Sci. U. S. A. 113 (2016) 13402–13407.
[37] K. Liu, J.E. Rehfus, E. Mattson, C.M. Kaiser, The ribosome destabilizes native and non-native structures in a nascent multidomain protein, Protein Sci. 26 (2017) 1439–1451.
[38] D.E. Segall, P.C. Nelson, R. Phillips, Volume-exclusion effects in tethered-particle experiments: bead size matters, Phys. Rev. Lett. 96 (2006), 088306.
[39] R. Kudva, P. Tian, F. Pardo-Avila, M. Carroni, R.B. Best, H.D. Bernstein, G. von Heijne, The shape of the bacterial ribosome exit tunnel affects cotranslational protein folding, elife 7 (2018), e36326.
[40] S.E. Leininger, F. Trovato, D.A. Nissley, E.P. O'Brien, Domain topology, stability, and translation speed determine mechanical force generation on the ribosome, BioRxiv (2018), https://doi.org/10.1101/490821.